Robustness of Turing models and gene regulatory networks with a sweet spot

Roozbeh H. Pazuki and Robert G. Endres
Department of Life Sciences, Imperial College, London SW7 2AZ, United Kingdom
and Center for Integrative Systems Biology and Bio-informatics, Imperial College, London SW7 2AZ, United Kingdom

(Received 17 July 2023; revised 29 February 2024; accepted 6 May 2024; published 11 June 2024)

Traditional linear stability analysis based on matrix diagonalization is a computationally intensive process for high-dimensional systems of differential equations, posing substantial limitations for the exploration of Turing systems of pattern formation where an additional wave-number parameter needs to be investigated. In this paper, we introduce an efficient and intuitive technique that leverages Gershgorin's theorem to determine upper limits on regions of parameter space and the wave number beyond which Turing instabilities cannot occur. This method offers a streamlined avenue for exploring the phase diagrams of other complex multi-parametric models, such as those found in gene regulatory networks in systems biology. Due to its suitability for the asymptotic limit of infinitely large systems, it predicts the existence of a sweet spot in network size for maximal Jacobian stability.

DOI: 10.1103/PhysRevE.109.064305

I. INTRODUCTION

Deciphering reproducible pattern formation during embryogenesis with multiparameter models calls for mechanisms demonstrating robustness in parameter space. Turing models of diffusion-driven instability [1], which serve as a pivotal category of models, only induce patterns within a highly restricted region of the parameter space [2–5]. The exploration of such models for increased regions of parameter space and hence enhanced robustness is markedly limited due to their inherent complexity: they incorporate numerous parameters, including rate constants and diffusion constants of activator and inhibitor morphogens, as well as a wave number parameter as part of the analysis.

Here, we consider autonomous spatiotemporal dynamic models that include diffusion, such as describing reaction-diffusion phenomena. Their partial differential equations (PDEs) are written as

$$\frac{d\boldsymbol{X}}{dt} = \boldsymbol{f}(\boldsymbol{X};\boldsymbol{\theta}) + \boldsymbol{D}\nabla^2\boldsymbol{X}, \tag{1}$$

where $\boldsymbol{X} \in \mathbb{R}^n$ are system variables, $\boldsymbol{f}$ is an n-valued function defined in n-dimensional phase space, $\boldsymbol{\theta} \in \mathbb{R}^m$ is the system-independent parameter vector, $\boldsymbol{D}$ is the diffusion matrix, and ∇^2 the Laplacian. One biologically inspired example is gene networks regulating embryonic development [3]. The concentration of proteins can affect the production of other proteins in the same or, via small messenger molecules, different cells. In fact, for n different proteins, the regulations' direction is represented by the edges of a directed graph, including self-loops for self-regulation. Typically, regulation is modeled by

$$f_i(\boldsymbol{X};\boldsymbol{\theta}) = b_i - \mu_i x_i + \prod_{j\in S_i} H(x_j), \quad i \in \{1,\dots,n\}, \tag{2}$$

with $\boldsymbol{\theta} = \{\boldsymbol{b}, \boldsymbol{\mu}, \dots\}$ such that the rate of change of species i depends on a basal rate b_i, a non-negative degradation rate μ_i, and a product of Hill functions $H(x_j)$ (to be defined later). Note that the multiplication runs over S_i, which is the set of species that regulate the species i and correspond to in-edges of the regulation network. Similarly, it represents a nonzero entry in the network's adjacency matrix.

For systems with diffusion-induced instability capable of producing patterns, one requires the system without diffusion to be stable. Hence, one needs to solve the system of equations

$$\boldsymbol{f}(\boldsymbol{X}^*;\boldsymbol{\theta}) = 0 \tag{3}$$

for a given $\boldsymbol{\theta}$ to find fixed points $\boldsymbol{X}^*$, and then by writing the $n \times n$ Jacobian matrix $\boldsymbol{J}_0|_{\boldsymbol{X}^*}$ of the system at $\boldsymbol{X}^*$ and studying its eigenvalues, classify the fixed point stability. However, finding the eigenvalues of a matrix is an $O(n^3)$ process, which is computationally challenging for high-dimensional phase spaces. The mentioned problem becomes more acute when considering that a candidate dynamical system can have some parameters that change the system's stability. In this case, we need to redo all the steps for every point in parameter space to study the dynamical system's characteristics, e.g., the bifurcation diagram.

Specifically, for our reaction-diffusion system with diffusion-induced instability, the Laplacian is removed by spatial Fourier transformation at the expense of an extra parameter, the wave number. Hence, the linear stability analysis must be applied for different wave numbers to specify the dominant wavelength that finally shapes the stationary solution [3]. For a diagonal diffusion matrix $\boldsymbol{D}$, the Jacobian for a given wave number, say k, is

$$\boldsymbol{J}(k) = \boldsymbol{J}_0|_{\boldsymbol{X}^*} - k^2\boldsymbol{D}. \tag{4}$$

Published by the American Physical Society under the terms of the Creative Commons Attribution 4.0 International license. Further distribution of this work must maintain attribution to the author(s) and the published article's title, journal citation, and DOI.

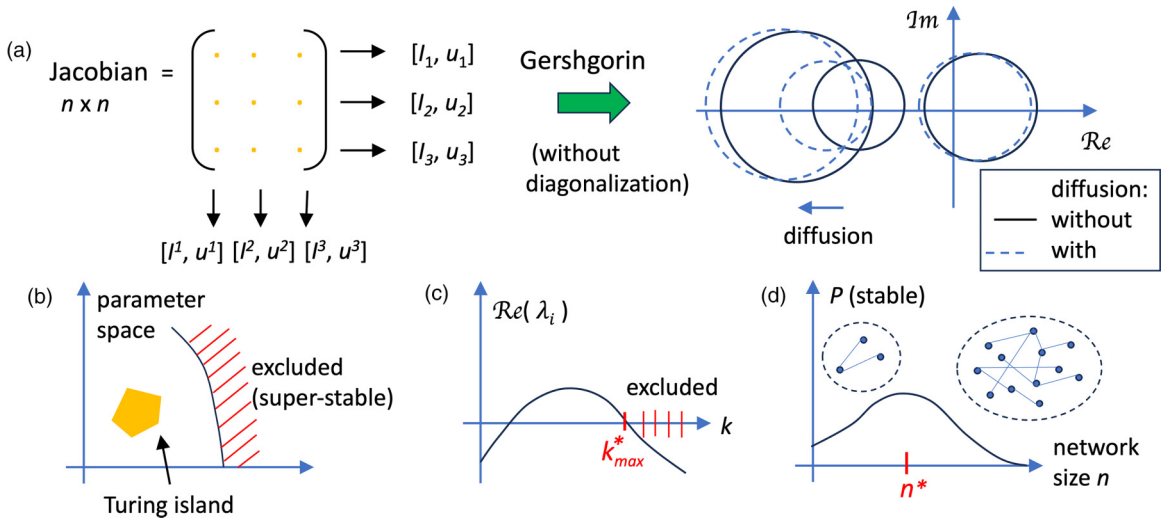


FIG. 1. Overview of our method to efficiently explore the parameter space of Jacobian matrices. (a) The Gershgorin circle theorem is used to extract information on the locations of the eigenvalues in the complex plane, in particular, to obtain bounds on the largest real part. Note diffusion shifts circles to the left. Such bounds can be used to analytically exclude areas in parameter space which cannot lead to Turing instabilities (superstable hatched area) (b), to derive the maximal wave number $k^*_{\max}$ beyond which stability sets (hatched line) in (c), and to explore optimal stability of random Jacobian matrices as a function of network (or matrix) size n. Here, n^* indicates the network size corresponding to the maximum of the probability of being stable. Insets illustrate small (left) and large (right) random gene regulatory networks.

Hence, any improvement that decreases the procedure's computational complexity is beneficial for general stability analysis, particularly for pattern formation study.

In this paper, we introduce an efficient and intuitive methodology based on the well-known Gershgorin's theorem [6,7] in linear algebra. For sparse matrices, our algorithm scales as $O(n)$ and hence transfers the computational bottleneck to $O(n^2)$ root-finding methods, such as the Newton method for the steady states (Fig. 1). Our method serves as an initial screening process to rule out extensive portions of the parameter space when searching for diffusion-driven instabilities, to be followed up by complementary methods such as the Busse balloon [8]. Our method, applicable numerically and analytically, markedly accelerates the parameter space exploration process [Figs. 1(a)–1(c)]. We illustrate the numerical efficacy of this approach using a two-morphogen model based on sigmoidal Hill functions, the Brusselator model [9], and large gene regulatory networks based on Eq. (2) using random matrix theory on Erdös-Rényi networks [Fig. 1(d)] [10] (for details, see Supplemental Material [11]). Note our method is markedly different from other recent work, such as provided in Refs. [12,13]. The former discusses discrete hopping on a network, while the latter derives conditions for pattern formation in systems valid for $n \geqslant 1$, but with the computational complexity being exponential and hence intractable for systems with many chemical species.

II. METHODS AND ALGORITHMS

A. Gershgorin's theorem

We start by introducing Gershgorin's theorem and consider its geometrical interpretation. As we shall see, it is possible to construct an algorithm that checks the rows or columns of a Jacobian matrix to find those that are unstable or remain stable after introducing diffusion and consequently cannot produce a diffusion-induced pattern. The theorem [6] states that for $n \times n$ complex matrix $A = (a_{ij})$ and $r_i \equiv \sum_{\substack{j=1 \\ j\neq i}}^{n} |a_{ij}|$, the sum of moduli of off-diagonal elements in the ith row, each union of circles $|z - a_{ii}| \leqslant r_i$ (for $i = 1, 2, \ldots, n$) contains a number of eigenvalues of A equal to the number of circles used to create the union. The analogous result holds if columns of A are considered. Note that in our case, $a_{ij} = \partial_i f_j$, and for diagonal terms $a_{ii} = \partial_i f_i$ without and $a_{ii} = \partial_i f_i - k^2 D_i$ with diffusion.

Let us consider the radius and position of a circle in the complex plane as depicted in Fig. 2. Depending on the sign of the diagonal term a_{ii}, the circle's center is on the real axis's negative or positive side. Assume λ_i lies in the Gershgorin circle belonging to the row or column i of the matrix A. Four types of circles may appear: Type 1: As shown in Fig. 2(a), we have $a_{ii} < 0$ and $h_i \equiv |a_{ii}| - r_i \geqslant 0$. Therefore, regardless of where the eigenvalue is inside the circle, its real part must be negative, $\mathrm{Re}(\lambda_i) \leqslant 0$. 2: In Fig. 2(b), we can see $a_{ii} < 0$, and the center of the circle is placed on the negative side of the real axis. However, since $|a_{ii}| < r_i$ and $h_i < 0$, the real part of λ_i can be negative or positive. In other words, the theorem is inconclusive about the sign of the real part of the corresponding eigenvalue. Type 3: The diagonal element is positive ($a_{ii} > 0$), and the center of the circle is on the positive side of the real axis. Yet, $|a_{ii}| > r_i$ and $h_i > 0$. Thus, the real part of the eigenvalue must be positive $\mathrm{Re}(\lambda_i) > 0$. Type 4: Similar to Type 2, the range of Gershgorin's circle spans from negative to positive values. Therefore, we cannot conclusively decide about the real part of the eigenvalue inside this area.

We must emphasize that when two or more Gershgorin's circles overlap, the eigenvalues lie in the union of the circles. Let us define the lower and upper bounds of each circle as

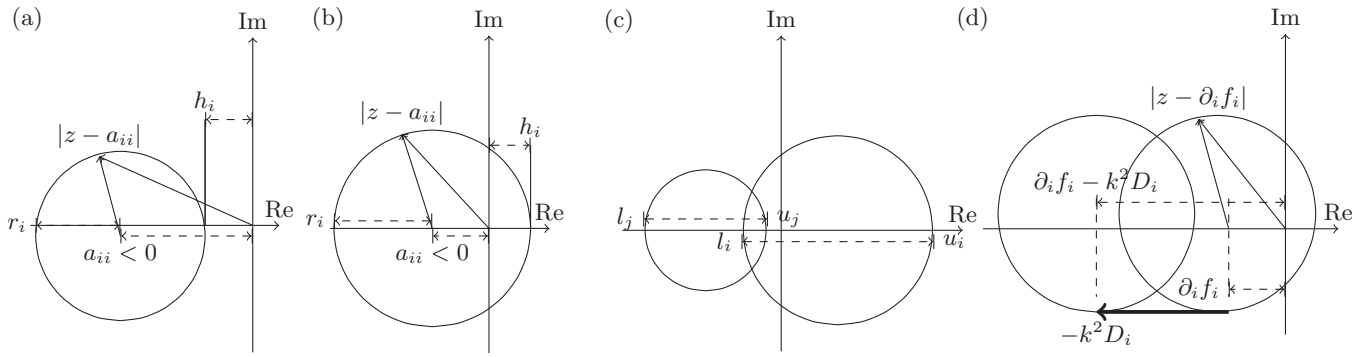


FIG. 2. Gershgorin's theorem and its geometrical interpretation. (a) Type 1 (stable). (b) Type 2 (inconclusive). (c) Two overlapping circles. (d) Diagonal terms shift to the left when diffusion is included.

$l_i \equiv a_{ii} - r_i$ and $u_i \equiv a_{ii} + r_i$, respectively. For instance, in Fig. 2(c), the union of two circles shows that the real part of both eigenvalues corresponding to rows i and j must be in the union of their diameters $\mathrm{Re}(\lambda_i), \mathrm{Re}(\lambda_j) \in [l_j, u_j] \bigcup [l_i, u_i] = [l_j, u_i]$. And, correspondingly, for each row (or column) of the matrix A, there exist intervals like

$$A = \begin{pmatrix} a_{11} & a_{12} & \dots & a_{1n} \\ a_{21} & a_{22} & \dots & a_{2n} \\ \vdots & & \ddots & \vdots \\ a_{n1} & a_{n2} & \dots & a_{nn} \end{pmatrix} \Rightarrow \begin{matrix} [l_1, u_1] \\ [l_2, u_2] \\ \vdots \\ [l_n, u_n], \end{matrix} \tag{5}$$

where after taking their unions and reformulating as nonoverlapping, disjoint intervals result in

$$\mathcal{A} = \bigcup_{i=1}^{n} [l_i, u_i] \equiv \bigcup_{i=1}^{p} [L_i, U_i], \qquad 1 \leqslant p \leqslant n, \tag{6}$$

such that $[L_i, U_i] \cup [L_j, U_j] = \emptyset$, for $i \neq j$. Therefore, the $[L_{\max}, U_{\max}]$ is the rightmost disjoint interval constructed by the unions of the original intervals and is sufficient to study it to find the sign of the real part of the largest eigenvalue. This introduces the following possibilities regarding the stability condition: (1) For $U_{\max} \leqslant 0$, the real part of the largest eigenvalue is negative. Consequently, the system is stable. (2) For $L_{\max} > 0$, the real part of the largest eigenvalue is positive. Consequently, the system is unstable. 3. For $L_{\max} \leqslant 0 < U_{\max}$, the situation is inconclusive.

At this stage, we can use the obtained results in two different ways. The first possibility is when the Jacobian is written in terms of the model's parameters, $\boldsymbol{\theta}$, and we may be able to derive the rightmost disjoint set parametrically. Accordingly, our inequalities define the regions in parameter space where the method can conclusively determine the stability or instability of the system. Nevertheless, the region corresponding to the inconclusive range requires different classification techniques. Note that even if the method is not always conclusive for all the regions in parameter space, it can always find a theoretical lower bound for the volume of the parameter space that the system is stable or unstable. The second possibility is when studying a system's linear stability numerically. We propose an algorithm that classifies a given Jacobian matrix into stable, unstable, and inconclusive stability groups (see Supplemental Material in Ref. [11]). The computational complexity of this algorithm is $O(n^2)$ [$O(n)$ for sparse matrices], making this comparable to iterative solvers [14]. However, due to its graphical interpretation and simple formalism, it is intuitive. Note that the algorithm can also be used for random matrices to find the average behavior of realistic systems or to study systems in the asymptotic thermodynamic limit for $n \to \infty$, which assumes the number of different constituent species is unbounded from above. Next, we include diffusion to make predictions about the ability of reaction-diffusion models to form patterns.

B. Effects of diffusion in reaction-diffusion models

To study pattern-forming systems based on Eq. (1) with stationary solution $\boldsymbol{X}^* = (X_1^*, \dots, X_n^*)$, we use our method to find bounds on the linear stability of the Jacobian $\boldsymbol{J}|_{\boldsymbol{X}^*}$ in Eq. (4). We can write the lower and upper bounds corresponding to row (or column) i as $l_i = \partial_i f_i - r_i$ and $u_i = \partial_i f_i + r_i$ for $r_i \equiv \sum_{j \neq i} |\partial_j f_i|$. Then, the stability (instability) criteria of the Jacobian determine the patterning conditions.

Next, we study the effect of introducing diffusion and derive bounds on maximally permissible wave numbers. For a given wave number k, the inclusion of diffusion shifts all the diagonal terms by $-k^2 D_i$ [see Eq. (4)]. Effectively, since diagonal terms correspond to the location of the centers of Gershgorin's circles, it is geometrically equivalent to saying all the circles shift to the left as shown in Fig. 2(d). Note, since the off-diagonal terms have not changed, the circles' radii remain unchanged.

Indeed, for any given circle partially on the positive side of the real axis, there exists a maximum shift by a wave number defined by $k_i^* = \sqrt{(r_i + \partial_i f_i)/D_i}$ that transfers the circle entirely to the negative side of the real axis by $k_i^{*2} D_i$—note that k_i^* is calculated for the diffusing species only (for details, see Supplemental Material in Ref. [11]). Furthermore, the real part of the eigenvalue corresponding to that circle must be negative for all the higher wave numbers $k_i > k_i^*$. By finding $k_{\max}^* \equiv \max\{k_1^*, \dots, k_n^*\}$ for all rows (or columns), the linear stability of different wave numbers can be restricted to the range k, such that for $k = 0$, or the case with no diffusion, $\boldsymbol{J}_0|_{\boldsymbol{X}^*}$ specifies the stability condition and $\boldsymbol{J}(k)$ for $k \in (0, k_{\max}^*]$ determines the evolution of the dominant wave number in a perturbed system. Thus, we must have three different regimes: (1) For $\boldsymbol{J}_0|_{\boldsymbol{X}^*}$, when $U_{\max} \leqslant 0$, all the circles are on the negative side of the real line and including diffusion

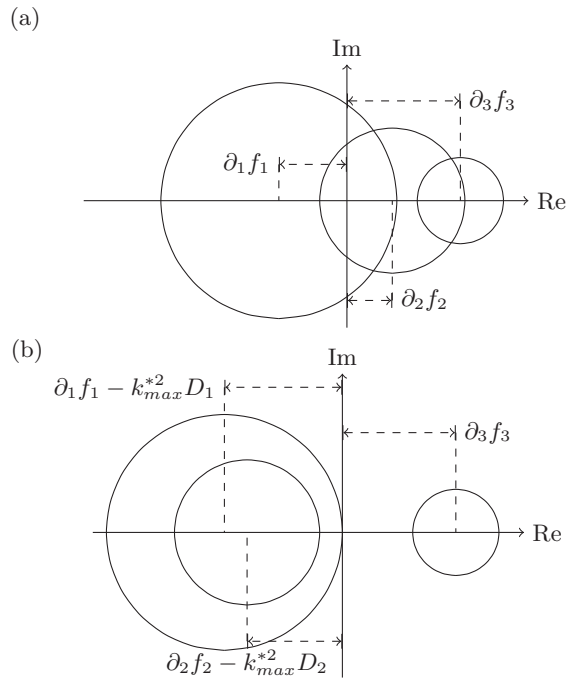


FIG. 3. Maximum shift of two diffusers. (a) Circles before inclusion of diffusion. (b) The maximum shifts of the first and second circles due to diffusion.

for any given wave number shifts the circles further to the left. Hence, all real parts of the eigenvalues are negative, and diffusion cannot excite any wave number. Consequently, the system is incapable of producing a diffusion-driven pattern (superstable). (2) On the contrary, when $L_{\max} > 0$ for $\boldsymbol{J}_0|_{\boldsymbol{X}^*}$, the initial stationary state is unstable and incapable of producing a pattern (unstable). (3) Finally, when $[L_{\max}, U_{\max}]$ is inconclusive ($L_{\max} < 0$ and $U_{\max} > 0$), $\boldsymbol{J}_0|_{\boldsymbol{X}^*}$ must be studied by finding its eigenvalues. And if one finds that it is stable, the maximum of the dispersion relation $\lambda(k)$ finds the dominant wave number for pattern formation by restricting k to $[0, k^*_{\max}]$. These regimes are included in our algorithm to speed up the process of checking the possibility of pattern formation for a given parameter set. Only parameters for which the classification is inconclusive need further study of their eigenvalues and are, in principle, able to form patterns.

C. Limitations

The dispersion relation of systems in which all species are diffusing always satisfies $\mathrm{Re}(\lambda(k)) < 0$ for $k > k^*_{\max}$. In other words, asymptotically, as long as all species are diffusers, we have $\lim_{k\to\infty} \mathrm{Re}(\lambda(k)) \to -\infty$. When some but not all species in a reaction-diffusion model diffuse, introducing the diffusion coefficients into the Jacobian matrix shifts some circles to the left while the others remain in the same place—see Fig. 3. Although one can calculate the $k^*_{\max}$ values for the diffuser rows in the matrix, a special situation can arise for $k > k^*_{\max}$ in the dispersion relation. For instance, consider that two of the three species are diffusers as shown in Fig. 3. As we can see, after shifting the diffusers' circle by an amount $-k^{*2}_{\max} D_1$ and $-k^{*2}_{\max} D_2$, respectively, the third eigenvalue corresponding to the nondiffuser element remains positive for all $k > k^*_{\max}$. Consequently, the real part of the dispersion relation can remain positive with no upper bounds. As a result, no dominant wave number exists to create a stationary pattern.

To overcome this limitation, note that the diffusing species' circles will eventually separate from the rest of the circles for large enough wave numbers. Therefore, a simple algorithm can reexamine the matrix with shifts $-k^{*2}_{\max} D_i$ included for all diffusing species. The classification is done for cases similar to Fig. 3 or stable matrices. Otherwise, if one or more nondiffusing species' circles are in an inconclusive region and the shifted diffusing circles overlap with them, the algorithm retries to increase $-(k^*_{\max} + \epsilon)^2 D_i$ for $\epsilon > 0$, until all diffusing circles are separated from the inconclusive ones, such that any excited wave number must be in $(0, k^*_{\max} + \epsilon]$. Note that this procedure always halts after separation of diffusing circles for some large enough ϵ, and the usual dispersion relation analysis can be carried out.

D. Tightening the bounds

Further improvements to our bounds can be made by isolating Gershgorin circles. Given an invertible matrix $\boldsymbol{D}$, $\boldsymbol{B} = \boldsymbol{DAD}^{-1}$ introduces an equivalence relation between square matrices $\boldsymbol{A}$ and $\boldsymbol{B}$ such that matrix $\boldsymbol{B}$ has the same eigenvalues as $\boldsymbol{A}$ (see Supplemental Material [11] for details). Defining an invertible $n \times n$ diagonal matrix $\boldsymbol{D}$ as the identity matrix with exception of matrix element $D_{ii} = 1/d_i$, the transformed matrix $\boldsymbol{DAD}^{-1}$ has the form

$$\boldsymbol{DAD}^{-1} = \begin{pmatrix} a_{11} & \dots & a_{1i}d_i & \dots & a_{1n} \\ \vdots & \ddots & \vdots & & \vdots \\ \frac{a_{i1}}{d_i} & \dots & a_{ii} & \dots & \frac{a_{in}}{d_i} \\ \vdots & & \vdots & \ddots & \vdots \\ a_{n1} & \dots & a_{ni}d_i & \dots & a_{nn} \end{pmatrix}. \tag{7}$$

The transformation's effect is similar to dividing all the elements of the row i by d_i and multiplying the elements of the column i by d_i. Consequently, the diagonal term a_{ii} remains the same.

Consider the rows of the resulting matrix. The radii of all circles corresponding to rows other than i expand by the amount $|a_{ji}|(d_i - 1)$ (for $d_i > 1$), and the ith radius shrinks by a factor of $1/d_i$, while the centers of all circles stay the same. Since the eigenvalues of the transformed matrix are the same as the original one, one can hope the shrunk circle becomes isolated from the rest since the expansions of the other radii are smaller than the shrinking of the single radius. In practice, one can find d_i that isolates the circle with the largest center from the rest. The interval of all rows except the ith is $[l_j, u_j] = [a_{jj} - |a_{ji}|(d_i - 1) - r_j, \quad a_{jj} + |a_{ji}|(d_i - 1) + r_j]$, and the interval for row i is $[l_i, u_i] = [a_{ii} - \frac{r_i}{d_i}, \quad a_{ii} + \frac{r_i}{d_i}]$.

To tighten the bounds, we have two distinct cases that can be studied separately. Case (1): When the diagonal term is positive, or $a_{ii} > 0$, to isolate the circle corresponding to row i, its leftmost point, or $l_i = a_{ii} - \frac{r_i}{d_i}$, must be larger than every other circle's rightmost point, or $u_j = a_{jj} + |a_{ji}|(d_i - 1) + r_j$. As explained in detail in Ref. [11], if all the rows j and

TABLE I. Empirical statistics of applying Algorithms (1) and (2) to the Hill-functions-based Turing model. Simulations are conducted for 10^9 parameter combinations.

	Total	Superstable	Inconclusive	Unstable	No fixed point
Row-wise	10^9	850 677 030	140 394 311	4 870 615	4 058 044
	100%	85.07%	14.04%	0.49%	0.41%
Columnwise	140 394 311	68 454 498	71 913 845	25,968	
	100%	48.76%	51.22%	0.02%	
Tighten bounds	71 913 845	64 615 611	6 990 298	307 936	
	100%	89.85%	9.72%	0.43%	
Combined	10^9	983 747 139	6 990 298	5 204 519	4 058 044
	100%	98.37%	0.70%	0.52%	0.41%

the largest one, i, satisfy the inequalities

$$\begin{cases} (a_{jj} - a_{ii} + r_j - |a_{ji}|)^2 & > & 4|a_{ji}|r_i & j \neq i \\ a_{jj} - a_{ii} + r_j - |a_{ji}| & < & 0 & j = 1, \ldots, n. \end{cases} \tag{8}$$

Simultaneously, there exists a d_i that isolates the rightmost eigenvalue, and the Jacobian is conclusively unstable. Case (2): When the largest diagonal term is negative, or $a_{ii} < 0$, the latter implies all the other diagonal terms are negative too. In this case, we search for a possible shrinkage value d_i, such that while the circle of the row i shrinks with its upper bound on the negative side of the real axis, the growth of all the other circles keeps them at the negative side. Combined, this leads to two conditioned bounds as

$$\frac{r_i}{|a_{ii}|} < d_i < \min_{j \neq i} \left(\frac{|a_{jj}| - r_j}{|a_{ji}|} + 1 \right). \tag{9}$$

Hence, if a nonempty interval can be found that satisfies the above inequalities, the Jacobian is conclusively "superstable" (see Supplemental Material [11] for details).

III. RESULTS AND APPLICATIONS

A. Numerical test on two-morphogen model

To test the fraction of rejections and, consequently, the speedup due to Algorithms (1) and (2), we use a biologically inspired model capable of producing Turing patterns [3] for two proteins (morphogens) in Eq. (2) with sigmoidal Hill functions and nine free parameters (see Supplemental Material [11]),

$$\begin{aligned} \frac{\partial u}{\partial t} &= b_u + \frac{V_u}{\left[1 + \left(\frac{K_{uu}}{u}\right)^4\right]\left[1 + \left(\frac{v}{K_{vu}}\right)^4\right]} \\ &\quad - \mu_u u + D_u \nabla^2 u, \\ \frac{\partial v}{\partial t} &= b_v + \frac{V_v}{1 + \left(\frac{K_{uv}}{u}\right)^4} - \mu_v v + D_v \nabla^2 v, \end{aligned} \tag{10}$$

with basal expression rates b_i, maximal expression rates V_i of regulated terms, thresholds K_{ij}, degradation rates μ_i, and diffusion constants D_i for $i, j \in \{u, v\}$. The Jacobian of the linearized form of the above equations is a 2×2 matrix, and, in practice, the computational cost of calculating its eigenvalues is not much different than our algorithm. However, we selected this model since the algorithm's correctness can be easily checked by comparing the determinant and trace of the Jacobian.

In this simulation, we selected 10^9 parameter combinations and applied Algorithm (1) to classify them into unstable, superstable, inconclusive, and no fixed point Note that no fixed point refers to the parameter combinations for which the root-finding algorithm could not find any stationary solutions. We first used our Algorithm (1) for a rowwise comparison and, after that, by using the inconclusive results from the first run, we used the algorithm again for a columnwise calculation. And, finally, we classified the remaining inconclusive cases using our Algorithm (2). These results are presented in Table I, showing that more than 99.3% of the parameter combinations were rejected. This provides an upper limit on the robustness of Turing patterns given a certain sampling of parameter space [3]. Using Ref. [3] as a baseline, the range of biologically relevant values for all parameters is $[10^{-2}, 500]$, except for the diffusion coefficients which are fixed to $D_u = 0.01$ and $D_v = 1$.

B. Brusselator model

Next, we searched for inequalities that separate the parameter space of the Brusselator model [9] into inconclusive and else. The Brusselator is a two-species reaction-diffusion model with a set of partial differential equations like

$$\begin{aligned} \frac{du}{dt} &= D_u \nabla^2 u + a - (b+1)u + u^2 v, \\ \frac{dv}{dt} &= D_v \nabla^2 v + bu - u^2 v \end{aligned} \tag{11}$$

for two parameters $a, b > 0$. Using the stability analysis, we can derive the Jacobian of the model at its fixed point $(u^*, v^*) = (a, b/a)$ as

$$\begin{array}{ccc} \begin{pmatrix} b-1 & a^2 \\ -b & -a^2 \end{pmatrix} & \Rightarrow [b-1-a^2, b-1+a^2] \\ \Downarrow \quad \Downarrow & \Rightarrow [-a^2-b, -a^2+b] \\ [-1, 2b-1] \quad [-2a^2, 0] & \end{array} . \tag{12}$$

After checking the sign of the circles' center, we find

$$\begin{cases} b > 1 + a^2 \\ a > 0, \end{cases} \qquad \begin{cases} b \leqslant 1 - a^2 \\ b \leqslant a^2 \end{cases} \tag{13}$$

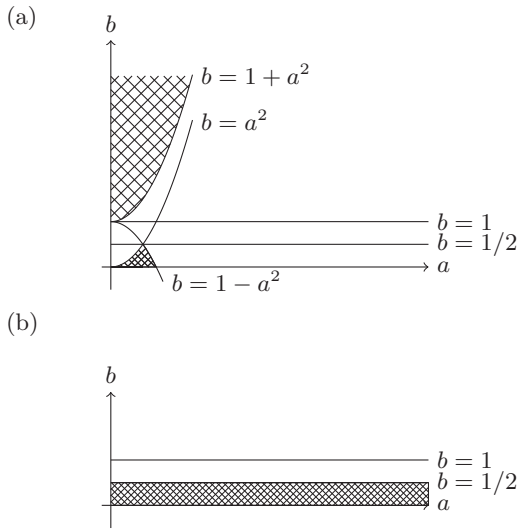


FIG. 4. Brusselator's parameter space. (a) Row-induced parts of the parameter space (hatched area) that cannot produce Turing patterns. (b) Analogous column-induced conclusive part of the parameter space (hatched area).

for the row constraints, shown in Fig. 4(a). Similarly, the conditions for the columns are written as $0 \leqslant b \leqslant 1/2$, as depicted in Fig. 4(b).

C. Large random gene regulatory networks

When constructing Jacobian matrices for systems without self-regulation using Eq. (2), we find that all the diagonal terms simply correspond to $-\mu_i$ from degradation, and off-diagonal entries are products of Hill functions and one of its derivatives at X^*. Specifically, defining the Hill functions as

$$H(u_j) \equiv \begin{cases} \frac{V_{ji}}{1+\left(\frac{K_{ji}}{u_j}\right)^{n_{ji}}} & \text{for activation} \\ \frac{V_{ji}}{1+\left(\frac{u_j}{K_{ji}}\right)^{n_{ji}}} & \text{for inhibition} \end{cases} \tag{14}$$

and furthermore

$$R \equiv \prod_{j \in S_i} H(u_j), \tag{15}$$

the off-diagonal terms are given by

$$\frac{dR}{du_k} = \frac{dH(u_k)}{du_k} \prod_{\substack{j \in S_i \\ j \neq k}} H(u_j). \tag{16}$$

By assuming diagonal and off-diagonal entries as independent random variables, we derive the lower bound probabilities of having a stable or a pattern forming random Jacobian. To this end, we assume a uniformly distributed range of biologically acceptable degradation rates between zero and c such that $\mu_i \sim U(0, c)$. Similarly, the sum of the absolute values of the off-diagonal terms are assumed to be distributed in a well-defined manner as $r_i \sim f_r(r)$.

A pattern-forming random Jacobian must be in the inconclusive regime, in which we denote its probability by $P_n(I)$ for a matrix with n species. Furthermore, given a matrix in the inconclusive regime, we denote the probability of having a stable Jacobian by $P_n(S|I)$. Finally, among all the stable inconclusive random matrices, the probability of having a pattern-forming dispersion relation with finite excitable wavelength is denoted by $P_n(U|I, S)$, given the matrix is inconclusive and stable without diffusion. Putting all together, the probability of having a pattern-forming random matrix is

$$P_n(\text{pattern}) = P_n(I)P_n(S|I)P_n(U|I, S). \tag{17}$$

Notice that the mentioned probability is constructed through conditionals to eliminate superstable and unstable matrices incapable of pattern formation.

To derive these conditional probabilities, we define

$$\alpha \equiv P(r < \mu), \tag{18}$$

as the probability of a single Gershgorin circle on the left side of the imaginary axis, and, similarly,

$$\gamma \equiv P(\text{Re}(\lambda) \geqslant 0) \tag{19}$$

as the probability of having a real non-negative eigenvalue, given the circle crosses the imaginary axis.

As the first result, we show that $0 < \alpha < 1$ (see Supplemental Material [11]), and consequently, the probability of obtaining a Jacobian in the inconclusive regime is

$$P_n(I) = 1 - P(r_1 < \mu_1, \ldots, r_n < \mu_n) = 1 - \prod_{i=1}^{n} P(r_i < \mu_i) = 1 - \alpha^n. \tag{20}$$

Asymptotically, we obtain

$$\lim_{n \to \infty} P_n(I) \to 1 \tag{21}$$

as expected due to the unavoidable crossing of the imaginary axis [Fig. 5(a)] .

Two simplifying assumptions are made for calculating $P_n(I)P_n(S|I)$: (1) Eigenvalues are equally probable to be everywhere inside the Gershgorin circle. (2) The probabilities of eigenvalues inside their circles are independent. Note that the reason that these are simplifying assumptions is that the locations of eigenvalues on the real axis are correlated. For example, the complex eigenvalues of a real matrix are a pair of complex conjugates, so their real parts are correlated. Also, two or more eigenvalues can be inside the union of Gershgorin circles while being entirely outside one of the circles. However, as we will see, these simplifications lead to a lower bound on the final probabilities.

Using these two assumptions, for a single circle the probability of crossing the imaginary axis is $(1 - \alpha)$ and of having an eigenvalue on the right side of the imaginary axis is γ. Given k out of n circles crossing the imaginary axis, the probability of all eigenvalues being on the left side of the imaginary axis (stable Jacobian) is

$$\binom{n}{k} \alpha^{n-k} (1 - \alpha)^k (1 - \gamma)^k. \tag{22}$$

The factor $(1 - \gamma)^k$ results from the assumed independence, which would be reduced for correlated eigenvalues. Furthermore, when calculating γ, the assumed uniform distribution underestimates its value since any nonuniformity

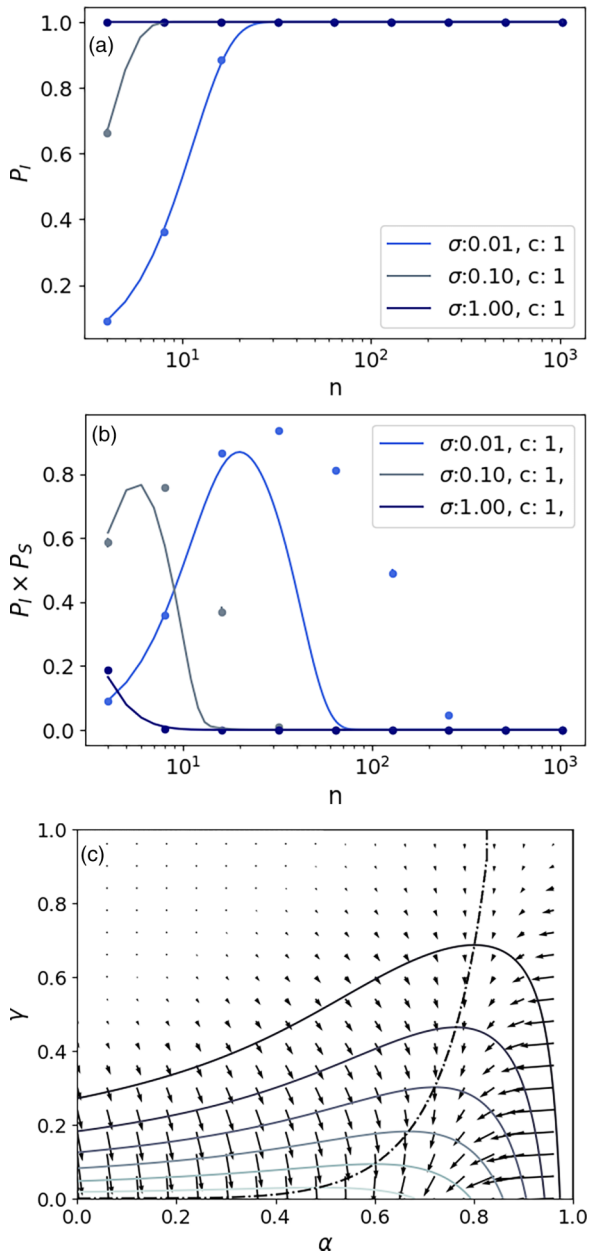


FIG. 5. Numerical estimates of $P_n(I)$, $P_n(I)P_n(S|I)$ and their lower bounds. $\mu_i \sim U(0, c = 1)$ and the off-diagonal entries are sampled from $\mathcal{N}(0, \sigma)$. Each dot is the averaged value of five ensembles of 1000 random matrices. The lines are the estimated lower bounds. (a) $P_n(I)$ and its lower bound. (b) $P_n(I)P_n(S|I)$ and its lower bound. (c) Contour and the gradient of $P_n(I)P_n(S|I)$ for $n = 6$. The domain of (α, γ) is divided into two parts by a dashed-dot line: from the right-side area toward the left-side one, the horizontal component of the gradient vectors changes the sign.

increases the integrals contained in Eq. (19). Hence, the lower bound of the probability of having an inconclusive and stable matrix is

$$P_n(I)P_n(S|I) \geqslant \sum_{k=1}^{n} \binom{n}{k} \alpha^{n-k}(1-\alpha)^k(1-\gamma)^k = [1-\gamma(1-\alpha)]^n - \alpha^n. \tag{23}$$

Further study of the last result shows that for increasing n, there is always a maximum probability–see solid lines in Fig. 5(b). In other words, a Goldilocks n^* exists for gene regulatory networks, and the probability of the system's stability is peaked at that size.

Apart from the general properties mentioned above, we wanted to investigate $\alpha(n)$ and $\gamma(n)$ and, consequently, $P_n(I)$ and $P_n(I)P_n(S|I)$ analytically and numerically. In Ref. [11], we derived two sets of results for when the off-diagonal terms are identically sampled from an exponential distribution or an arbitrary distribution that satisfies the condition for the central limit theorem. In the former case, $f_r(r)$ is the Erlang distribution and is exact for all ns, while in the latter, the estimates are accurate for larger enough n. Figure 5 shows the probabilities $P_n(I)$ and $P_n(I)P_n(S|I)$ of numerically sampled matrices. To construct these random matrices, μ_i is sampled from $U(0, c = 1)$ and the off-diagonal entries from a normal distribution $\mathcal{N}(0, \sigma)$. As we can see, the $P_n(I)$ estimate is exact [Fig. 5(a)], while $P_n(I)P_n(S|I)$ is a lower bound [Fig. 5(b), which is very close to the sampled values for small n but deviates for larger ones.

D. Role of self-regulation in stability

Having self-regulation leads to the inclusion of a new term in the diagonal matrix elements. To isolate the effect of self-regulation, we keep all parameters the same, e.g., for a given matrix size n, maximal degradation rate c, and constant mean and standard deviation of the off-diagonal terms, we are able to compare the probabilities $P_n(I)$ and $P_n(I)P_n(S|I)$ with and without self-regulation. Observe that the multiplicative terms in Eq. (16) are everywhere positive and, consequently, the sign of dR/du_k depends solely on the sign of dH/du_k, which is positive (negative) for activating (inhibiting) Hill functions. Accordingly, including self-inhibition adds a negative value to the diagonal term or, equivalently, shifts the center of the circle toward minus infinity. Conversely, including self-activation adds a positive value to the diagonal term and shifts the circle's center toward the imaginary axis. In the Supplemental Material [11], we show that

$$P_n(I|\text{self-inhibition}) \leqslant P_n(I|\text{no self-regulation}) \leqslant P_n(I|\text{self-activation}), \tag{24}$$

which means including self-activation (self-inhibition) increases (decreases) the probability of having an inconclusive matrix.

At the same time, depending on which part of the (α, γ) domain the model is in, self-activation and self-inhibition affect the $P_n(I)P_n(S|I)$ differently. For instance, in Fig. 5(c) the domain is divided into two regions (shown by a dash-dot line): (1) In the left-side area, self-activation (self-inhibition) always decreases (increases) $P_n(I)P_n(S|I)$. In other words, they act in opposite directions. (2) In the right-side area, the change of $P_n(I)P_n(S|I)$ depends on the model parameters. Note that for increasing values of n, the left-side area grows. The results are in agreement with the numerically sampled simulations, as explained in the Supplemental Material [11].

IV. CONCLUSIONS

We have introduced an efficient and intuitive method that uses Gershgorin's theorem to define robustness bounds in dynamical systems, particularly beneficial for reaction-diffusion models such as diffusion-driven Turing systems [3]. This approach can eliminate unstable, nondiffusive cases or solutions that remain stable postdiffusion while also setting an upper limit for wave numbers capable of pattern formation. When applied to specific models, our method not only enhances the speed of numerical algorithms but also facilitates an analytical study of parameter space. The method's utility and power increase significantly when accounting for parameters that alter the behavior of a potential dynamical system, and large networks as encountered in gene regulation. For the latter, it predicts the existence of a sweet spot in network size for maximal Jacobian stability.

While providing a number of powerful tools for constraining and excluding regions in parameter space, our study opens a range of new questions worth exploring in the future. First, we predict a sweet spot, but its exact value and interplay with sparsity and correlations among matrix elements are still largely unknown [15]. Second, investigating the probability P_n(pattern) remains to be done, although its value depends on the derived lower bounds of $P_n(I)P_n(S|I)$ and $P_n(U|I,S)$, and it must be peaked at some n value after multiplication, see Ref. [16]. We also derived $\alpha(n)$ and $\gamma(n)$ with random sparsity in the gene regulatory network. However, investigating its effect on the location of the maximum and its interplay with other parameters is left for future study. Third, in the special case when all the degradation rates are equal, the well-known circular law can be used to study the stability problem [17]. In this case, all the Gershgorin circles have the same center, and their radii grow as $n\mathbb{E}[r]$, while the circular law predicts that the eigenvalues are inside a circle with radius $\sqrt{n}\mathbb{E}[r]$ [15,18,19]. Therefore, the eigenvalues must be concentrated more densely toward the center of the Gershgorin circles. This observation can further reduce the underestimation of the current results in future work.

In conclusion, our method helps explore high-dimensional parameter spaces of dynamical systems for investigations of stability, even in the asymptotic limit. For instance, we showed that analytically $P_n(I)P_n(S|I) \to 0$ for $n \to \infty$. This result guarantees the eventual diminishing effect of including more distinct species in the system. In some sense, the idea of having a sweet-spot size of the system is based on the fact that the probabilities are zero for $n = 1$ (corresponding to a single species with $P_1(I) = 0$) and $n \to \infty$, resulting in a peak in between. The method is especially useful for spatiotemporal models with additional wave number dependence.

The implementation of the algorithms and the code to reproduce the plots in Python programming language are accessible through GitHub [20].

ACKNOWLEDGMENTS

We acknowledge support from the AI-4-EB Consortium for Bioengineered Cells and Systems (BBSRC Award No. BB/W013770/1).

[1] A. M. Turing, Phil. Trans. R. Soc. Lond. B **237**, 37 (1952).
[2] P. Maini, T. Woolley, R. Baker, E. Gaffney, and L. S. Seirin, Interface Focus **2**, 487 (2012).
[3] N. S. Scholes, D. Schnoerr, M. Isalan, and M. P. Stumpf, Cell Syst. **9**, 243 (2019).
[4] P. A. Haas and R. E. Goldstein, Phys. Rev. Lett. **126**, 238101 (2021).
[5] T. Woolley, A. Krause, and E. Gaffney, Bull. Math. Biol. **83**, 41 (2021).
[6] H. E. Bell, Am. Math. Mon. **72**, 292 (1965).
[7] R. S. Varga, *Geršgorin and His Circles*, Springer Series in Computational Mathematics Vol. 36 (Springer, Berlin, 2004).
[8] M. C. Cross and P. C. Hohenberg, Rev. Mod. Phys. **65**, 851 (1993).
[9] I. Prigogine and G. Nicolis, Self-organisation in nonequilibrium systems: Towards a dynamics of complexity, in *Bifurcation Analysis: Principles, Applications and Synthesis*, edited by M. Hazewinkel, R. Jurkovich, and J. H. P. Paelinck (Springer Netherlands, Dordrecht, 1985), pp. 3–12.
[10] U. Alon, *An Introduction to Systems Biology: Design Principles of Biological Circuits*, Chapman and Hall/CRC Computational Biology Series (CRC Press, United Kingdom, 2019).
[11] See Supplemental Material at http://link.aps.org/supplemental/10.1103/PhysRevE.109.064305 for additional derivations, algorithms, benchmarking, scaling, and results, which includes Ref. [20]. See also Ref. [21] for the Lengyel-Epstein model that is discussed there.
[12] Q. Zheng, J. Shen, and Y. Xu, Phys. Rev. E **102**, 062215 (2020).
[13] E. Villar-Sepúlveda and A. R. Champneys, J. Math. Biol. **86**, 39 (2023).
[14] Y. Saad, *Numerical Methods for Large Eigenvalue Problems*, 2nd ed. (Society for Industrial and Applied Mathematics, University of Minnesota, Twin Cities, 2011).
[15] S. Allesina and S. Tang, Population Ecology **57**, 63 (2015).
[16] In separate, unpublished work on random matrices, we have observed that the probability of having a Turing pattern has a peak as a function of n.
[17] M. Potters and J. Bouchaud, *A First Course in Random Matrix Theory: For Physicists, Engineers and Data Scientists* (Cambridge University Press, United Kingdom, 2020).
[18] R. May, Nature (London) **238**, 413 (1972).
[19] L. Stone, Sci. Rep. **8**, 8246 (2018).
[20] https://github.com/Endres-group/Gershgorin.
[21] I. Lengyel, G. Rabai, and I. R. Epstein, J. Am. Chem. Soc. **112**, 9104 (1990).